

# Assessment of flow-assisted corrosion rate of copper alloy cooling tube for application in fusion reactors

Johan Öijerholm<sup>a,\*</sup>, Chris Harrington<sup>b</sup>, Peter Gillén<sup>a</sup>, Allan Harte<sup>b</sup>, Liberato Volpe<sup>b,c</sup>, Jeong-Ha You<sup>d</sup>

<sup>a</sup> Studsvik Nuclear AB, 611 82 Nyköping, Sweden

<sup>b</sup> UK Atomic Energy Authority, Culham Centre for Fusion Energy, Abingdon, Oxon OX14 3DB, UK

<sup>c</sup> Materials Performance Centre, Department of Materials, The University of Manchester, Oxford Road, Manchester M13 9PL, UK

<sup>d</sup> Max Planck Institute for Plasma Physics, Boltzmann Str. 2, 85748 Garching, Germany

## ARTICLE INFO

### Keywords:

Fusion reactor  
ITER  
DEMO  
CuCrZr  
Flow-assisted corrosion

## ABSTRACT

In-vessel plasma facing components in fusion reactors such as ITER and DEMO experience high thermal loads and require active cooling, for which water is one possible coolant. The solution where plasma facing components utilise tungsten blocks as sacrificial armour has a joint internal structure of cooling tubes made from the copper base (~99 % Cu) alloy CuCrZr. This paper concerns the testing of CuCrZr tubes with respect to flow-assisted corrosion (FAC) at water velocity in the range 8–10 m/s and temperature in the range 150 °C–250 °C. The FAC rate was evaluated by gravimetry, microscopy, and sampling of the water from the re-circulating test system. When the electrochemical potential of the CuCrZr specimens was kept in the reducing range where Cu is thermodynamically stable as a metal, no FAC could be observed on the specimens. At electrochemical potentials that promotes oxidation of Cu through presence of an oxidizer the FAC rate of a straight CuCrZr tube was estimated to be in the order of 400 μm per full power year.

## Introduction

In fusion reactors, such as ITER and the DEMONstration Power Plant (DEMO), the tokamak concept is adopted in which a burning plasma is magnetically contained in a torus-shaped vacuum vessel. The in-vessel plasma facing components (PFCs) experience high thermal loads and require active cooling, for which water is one possible candidate. For the divertor targets, the solution where PFCs utilise tungsten blocks as sacrificial armour has an internal joint cooling structure in form of long tubes made of a copper base (~99 % Cu) alloy CuCrZr [1–5]. A schematic of a divertor PFC including a portion of the CuCrZr cooling tubes (Fig. 1-inset) is shown in Fig. 1.

For DEMO divertor PFCs utilizing CuCrZr heat sinks, bulk cooling water temperatures in the range of 130–150 °C, and local water temperatures of 250 °C or above are foreseen [3,6]. Coolant velocities in the CuCrZr heat sinks are planned to be around 14 m/s in order to remove heat at a sufficient rate from the sacrificial armour [3,7]. This very high flow velocity leads to significant risks of flow-assisted corrosion (FAC) within the CuCrZr tubes. Previous testing under conditions that

corresponded to those expected in a PFC observed rapid rates of FAC using jet impingement [8]; however the database of FAC behaviour of the CuCrZr alloy, particularly under a meaningful range of chemical and hydraulic conditions, remains sparse.

The water chemistry specifications for the heat transfer systems in DEMO is being actively developed [7]. During plasma operation the PFCs will experience heat fluxes up to 10 MW/m<sup>2</sup> in normal operation [5]. In addition, the PFCs will be subjected to neutron radiation (14 MeV), which generates gamma radiation through nuclear excitation within the PFCs themselves. Importantly, the high energy neutron flux significantly exceeds what is observed in a pressurized water reactor (PWR) [9]. There will thus be a strong tendency for forming oxidising radiolysis products such as H<sub>2</sub>O<sub>2</sub> and O<sub>2</sub> in the coolant, that can enhance FAC. To suppress radiolysis formation and corrosion in general, a hydrogenated water chemistry is proposed, and impurity limits are considered necessary, similar to what is adopted in light water reactors [7]. It is, however, uncertain whether H<sub>2</sub> additions will be sufficient to suppress completely the formation of oxidising species through radiolysis in the coolant. For instance, complete suppression of H<sub>2</sub>O<sub>2</sub> to sub-

\* Corresponding author.

E-mail address: [johan.oijerholm@studsvik.com](mailto:johan.oijerholm@studsvik.com) (J. Öijerholm).

<https://doi.org/10.1016/j.nme.2023.101433>

Received 14 December 2022; Received in revised form 6 April 2023; Accepted 8 April 2023

Available online 10 April 2023

2352-1791/© 2023 The Authors. Published by Elsevier Ltd. This is an open access article under the CC BY-NC-ND license (<http://creativecommons.org/licenses/by-nc-nd/4.0/>).

ppb levels in cooling channels of PFCs have proven to be difficult in fusion reactors, based on radiolysis modelling [10,11]. For this reason, testing of FAC of the CuCrZr alloy of the divertor PFCs is required over a range of chemical and hydraulic conditions in order to understand the dependency of lifetime degradation risks. This can then be used to refine the necessary water chemistry specification for the DEMO coolant loops and to identify any further mitigations required, such as the needs for protective anti-corrosion coatings [5].

This paper describes the use of an experimental set-up to expose reactor-relevant tube specimens of CuCrZr alloy to flowing water conditions with different chemistries and configurations. Exposure conditions and geometries representative of the latest DEMO divertor target design were chosen, and exposures were carried out at different temperatures. The electrochemical corrosion potential (ECP) during the exposures was either reducing (*i.e.*, Cu is thermodynamically stable as a metal) or oxidising (*i.e.*, Cu is thermodynamically stable in an oxidized state). The effect of the turbulence-promoting swirl tape is also investigated by including exposure of specimens both with and without the tape installed. Enhanced turbulence might potentially increase the rate of FAC by promoting the dissolution of otherwise protective oxide films. The results of this study will be used to enrich the FAC database for the CuCrZr alloy exposed under conditions similar to those expected for plasma facing components in DEMO.

## Experimental

### Specimen material

The specimen material was acquired in the form of a CuCrZr tube section manufactured by KME Germany GmbH & Co. KG. Specimens were machined from this material without further treatment except rinsing in acetone using an ultrasonic bath. The tubes had an outer diameter of 15 mm and an inner diameter of 12 mm, which is identical to the heat sinks intended for the DEMO divertor. The chemical composition and the principal mechanical properties of the specimen material are shown in Table 1.

**Table 1**

Chemical composition (wt. %) and mechanical properties of CuCrZr specimen tube.

Alloy composition			Mechanical properties			
Cr (wt. %)	Zr (wt. %)	Cu (wt. %)	Yield strength 0.2 % (MPa)	Tensile strength (MPa)	Elongation after fracture (%)	Hardness (HBW)
0.82	0.09	Bal.	514	546	21	159

### Experimental setup

The specimens were exposed in the re-circulating loop system, Studsvik High Flow velocity Loop (SHFL), that is capable of performing FAC testing under high flow velocity conditions at elevated temperature with control of the water chemistry. A schematic of the SHFL is shown in Fig. 2. A pump is used to re-circulate water at elevated temperature in a loop at a rate of up to 5 m<sup>3</sup>/h. The recirculating mass flow in the loop is obtained by using the ISO 5167 2003 standard where the measured differential pressure over an orifice is used as an input parameter. The re-circulation pump can operate at elevated temperature, but not provide the necessary pressure in the loop to suppress boiling. The pressure in the main loop is instead generated by a secondary pump which continuously injects a flow at comparatively low rate, 5–10 L/h into the primary loop. The injected high-pressure flow is also used to inject chemicals (*e.g.*, H<sub>2</sub>O<sub>2</sub> or dissolved gasses, such as O<sub>2</sub> and H<sub>2</sub>) in the main flow. A bleed flow at the same rate is diverted from the main loop to maintain mass balance. The bleed flow is used for controlling the pressure in the main loop, using a back pressure regulator (BPR), and monitoring the water chemistry by measurements of conductivity and the content of H<sub>2</sub> and O<sub>2</sub>. The water supplied to the loop is degassed ultra-pure water (UPW). Build-up of impurities in the water circulating in the main loop is suppressed, since part of the volume ( $\approx 40$  L), is continuously renewed by fresh UPW. The FAC testing is conducted in a dedicated section connected to the SHFL system, as shown in Fig. 2. Thus, the test section is continuously fed with fluid from the loop.

The specimens were mounted in the FAC test section using a tube-in-tube solution which allows the specimen to be exposed only to water of

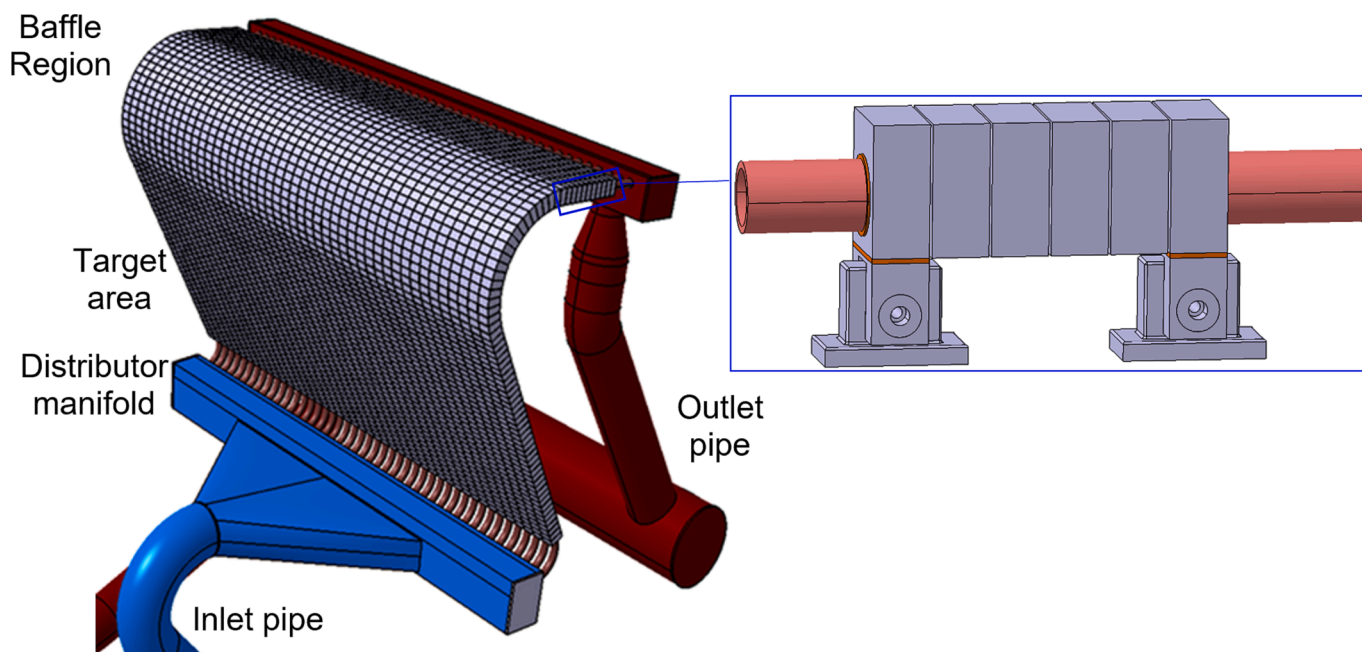


**Fig. 1.** Vertical target from a DEMO divertor cassette. The enlarged image to the right depicts a tungsten monoblock with an internal CuCrZr cooling tube. The illustration is based on reference [5], with permission from Elsevier.

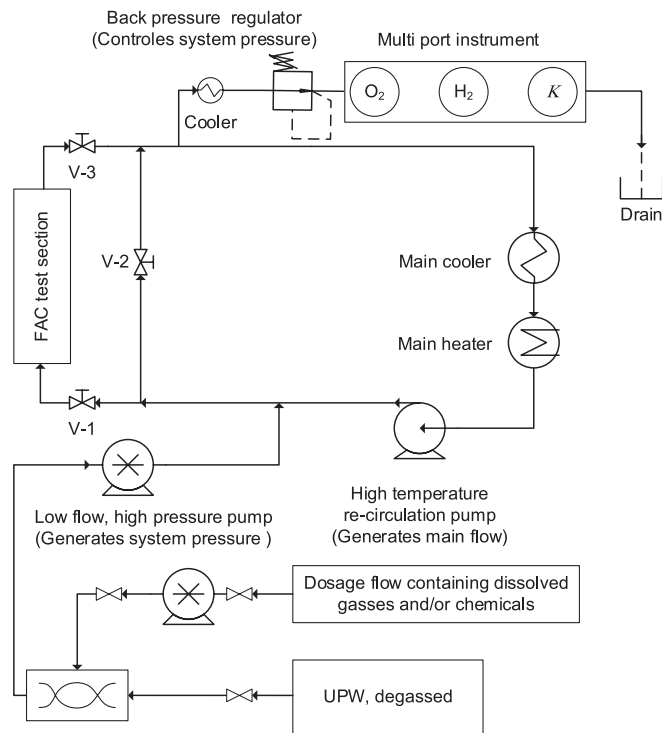


Fig. 2. Schematic illustration showing the setup used for FAC testing.

high flow velocity on the inside. An outer stainless steel tube serves as pressure boundary. Fig. 3 shows an overview of the test section and setup for exposure of a 100 mm long CuCrZr alloy tube. The CuCrZr alloy tube is placed in between two stainless steel guide tubes. The assembly of the stainless steel guide tube and the CuCrZr alloy tube is then inserted in the stainless steel pressure boundary tube. The assembly is kept in position with a hold down spring. Finally, the stainless steel pressure boundary tube is attached to the loop using tube fittings.

Tube sections with a swirl tape inserted for increased turbulence

were also tested. The function of the swirl tape is to increase turbulence and thus increase heat transfer from the tungsten armour of the divertor to the cooling water circulating in the CuCrZr tubes [3–6,12]. Fig. 4a shows a photo of a CuCrZr cooling tube and a swirl tape before assembly. During exposure, a stainless steel anchoring section was used to fix the swirl tape inside the CuCrZr cooling tube. The swirl tape itself was made of 99.95 % pure copper type EN Cu-OF/CW008A. Fig. 4b shows schematically how CuCrZr specimens, both without and with swirl tapes inserted, were assembled in the test section.

Analytical techniques

The general corrosion behaviour and FAC of the CuCrZr alloy tubes were evaluated after exposure with different and complementary techniques.

The FAC rate of the specimens was evaluated by gravimetry. Weighing of the specimens was performed prior and after exposure of the specimen using an analytical balance, KERN ABT 120–5-DM. The reproducibility of the balance is 0.01 mg, and all measurements were repeated three times and an average value was used in the subsequent analysis. Based on the calculated mass loss, the exposed inner surface area of the specimen and exposure time an average FAC rate was calculated based on a few assumptions:

- Weight loss due to FAC is evenly distributed over the exposed inside of the specimen tube. Thus, the outside of the tube is un-affected since the flow was stagnant in this area.
- Eventual corrosion film on the inside of the specimen is anticipated to be very thin (nanometre scale) [8], and its weight can be neglected.
- The density of the removed material was assumed to be equal to that of Cu ( $\rho_{Cu} = 8.96 \text{ g/cm}^3$ )

The level of dissolved corrosion products in the effluent from SHFL was monitored by grab sampling, and then the samples were analysed by inductively coupled plasma mass spectrometry (ICP-MS). The reporting limits for the analysis of metallic species were in the range of 0.01 to 0.2 ppb.

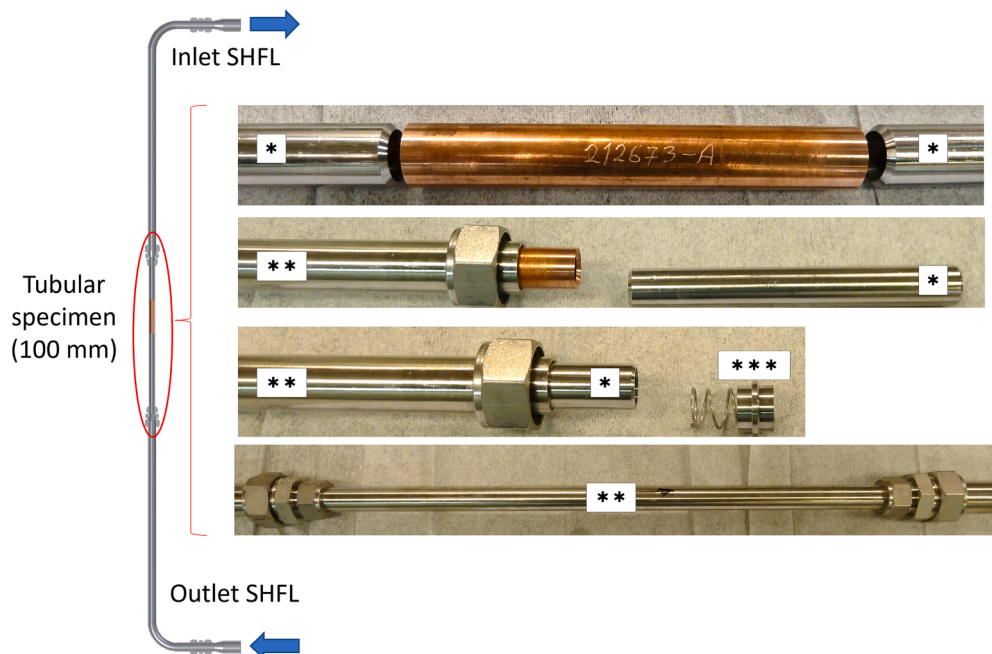
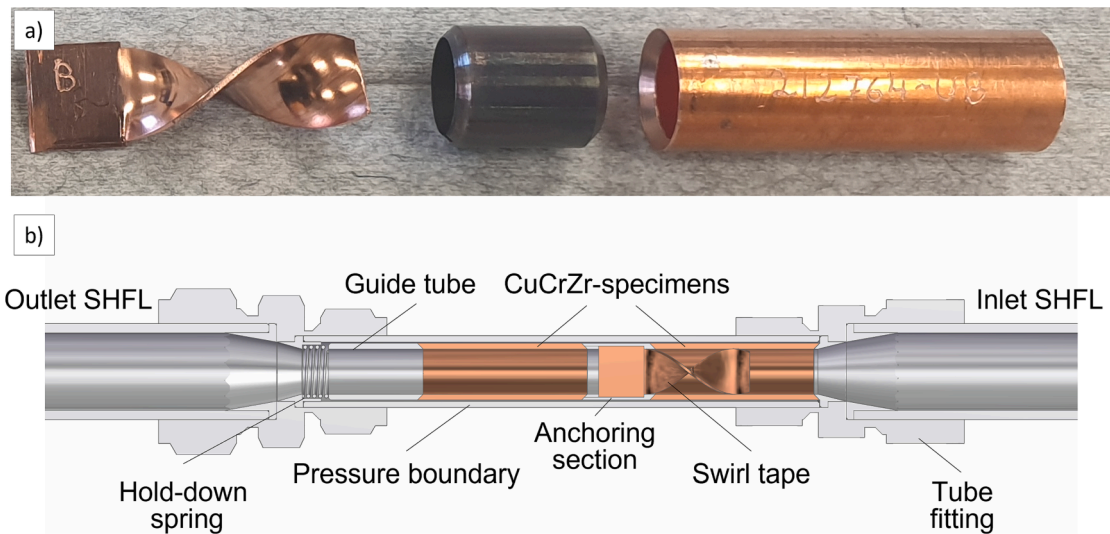


Fig. 3. To the left is an illustration of the test section which is approximately 1.5 m tall. The enlargement to the right shows how a CuCrZr alloy tube is loaded into the test section. The components correspond to: “\*” stainless steel guide tubes, “\*\*” stainless steel tube acting as pressure boundary and “\*\*\*” hold-down spring.



**Fig. 4.** (a) Photo of a swirl tape and its stainless steel 316L anchoring section along with the tubular CuCrZr specimen. (b) Schematic image of a simultaneous exposure of CuCrZr specimens without and with a swirl tape inserted.

A stereo microscope WILD heerbrugg M5 equipped with a leica DFC 295 camera was used to examine the sample surfaces prior and post exposure.

Scanning Electron Microscopy (SEM) imaging and energy dispersive X-ray spectroscopy (EDX) was performed with a Zeiss EVO LaB<sub>6</sub> to analyse the bulk metal, the surface oxide and the morphology and composition of secondary phases. Imaging was performed with a secondary electron (SE) detector at 8 keV and 500 pA, and with a working distance of 6.5 mm. SEM-EDX analyses were performed at 20 keV and 15 nA, with a working distance of 8.5 mm, using an Oxford Instruments (OI) windowed silicon drift detector (SDD) Ultim max 40. All analysis of chemical maps was performed with the raw counts and no attempt was made at chemical quantification. Further analyses were performed with a field emission gun (FEG) – SEM TESCAN Mira equipped with an OI SDD X-Max 80.

A dual-beam focus ion beam (FIB) Helios 660 Nanolab was used to obtain site-specific cross sections in order to analyse the near surface region of the specimens exposed under reducing conditions. Each site-specific region was protected with a layer of Pt equal to  $15 \times 1 \times 1 \mu\text{m}^3$  to avoid any interaction with the CuCrZr alloy surface and the Ga<sup>±</sup> beam during the FIB cross section preparation. SEM-EDX point “spot” analyses were performed to obtain qualitative data on the specimen exposed under reducing conditions and were performed with a live time of 60 s and a process time of 5 s with the specimen oriented perpendicular to the electron beam. The data were then analysed with the software OI Aztec (ver. 5.0) and plotted using Matplotlib (ver. 3.6.0) [13].

#### Exposure conditions

The focus of the exposure tests was to investigate the influence of temperature and ECP on FAC of CuCrZr tubes. Two different temperatures of the recirculating water in SHFL were chosen to represent the baseline options for the DEMO divertor system in different exposures: 150 °C to represent the bulk coolant conditions and 250 °C to capture the effect of local hot spots inside the cooling tubes. The ECP was chosen as either reducing or oxidising for the exposure tests. A reducing water chemistry, ECP at  $\approx -600$  mV SHE, was achieved by adding H<sub>2</sub> to the degassed feed water for SHFL. Oxidising conditions were achieved by injection of either H<sub>2</sub>O<sub>2</sub> or O<sub>2</sub>. It is worth noting that H<sub>2</sub>O<sub>2</sub> is a primary radiolysis product, and in fact H<sub>2</sub>O<sub>2</sub> can easily decompose into H<sub>2</sub>O and

O<sub>2</sub>. The decomposition is heterogeneously catalysed by metallic surfaces [14].

The ECP calculation of a metallic surface in contact with water containing H<sub>2</sub>O<sub>2</sub>, O<sub>2</sub> and H<sub>2</sub> is not straightforward, and it is necessary to consider both the thermodynamics and the kinetics of the reactions involved. A model which describes the ECP of a Cu-surface under such conditions at elevated temperatures and flow velocities was not available when the exposure was defined. However, for stainless steel there are several models available, such as the Studsvik’s ECP-model [14]. There are substantial differences between the electrochemical properties of stainless steel and Cu, e.g., stainless steel is oxidized under H<sub>2</sub> evolution by water, also at neutral pH. In Fig. 5 the effect on the ECP inside a stainless steel tube exposed to degassed ultrapure water containing either O<sub>2</sub> or H<sub>2</sub>O<sub>2</sub> is illustrated. The geometry of the tube is the same as the CuCrZr specimen and flow velocity and temperature are representative of the test conditions. From Fig. 5, it is clear that the overall ECP is mainly dominated by H<sub>2</sub>O<sub>2</sub> and not O<sub>2</sub>, and that sub-ppb levels of H<sub>2</sub>O<sub>2</sub> (>0.03 ppb) are sufficient to significantly elevate the ECP of stainless steel. Though the electrochemical properties are different between Cu and stainless steel, it is justifiable to assume that the general trends are similar as shown in Fig. 5, i.e., it is assumed that the ECP for Cu is mainly controlled and elevated by H<sub>2</sub>O<sub>2</sub> already at ppb levels.

Note that the oxidation of Cu in pure water in the temperature range 150 °C to 250 °C occurs at an ECP interval in between  $-130$  mV to  $-210$  mV with respect to the standard hydrogen electrode (SHE) scale [15,16]. For exposure at 150 °C, H<sub>2</sub>O<sub>2</sub> was injected to create an oxidising water chemistry. The steady state concentration of H<sub>2</sub>O<sub>2</sub> was estimated to be higher than 100 ppb [14] inside the loop during the exposure. Oxidising conditions were also verified by measuring the O<sub>2</sub> concentration due to decomposition of H<sub>2</sub>O<sub>2</sub> in the effluent from the SHFL. At 250 °C the decomposition rate of H<sub>2</sub>O<sub>2</sub> is very rapid and O<sub>2</sub> was injected directly instead to achieve oxidising conditions, see Fig. 5.

The flow velocity inside the CuCrZr specimens was maintained in the range of 8 to 10 m/s during the overall exposure. The limiting factor was the pressure drop created by the specimens mounted in the recirculating loop, especially from those fitted with swirl tape exposed at 250 °C.

In summary, one exposure test was performed under oxidising conditions at 150 °C, in which only a straight section of a CuCrZr tube was exposed (Table 2). Two exposure tests were performed at 250 °C under oxidising (Table 3) and reducing (Table 4) conditions. In both cases, the CuCrZr tubes were exposed with and without the internal swirl tape.

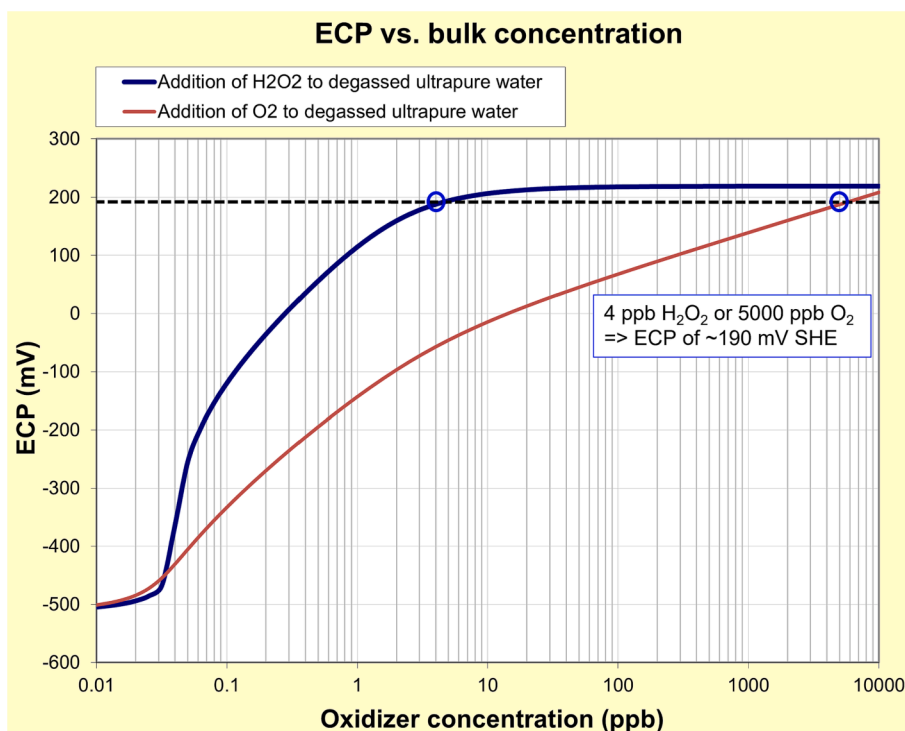


Fig. 5. Estimated ECP in a stainless steel tube with an inner diameter of 12 mm exposed at 250 °C to otherwise degassed ultrapure water with flow velocity of 10 m/s containing either O<sub>2</sub> or H<sub>2</sub>O<sub>2</sub>. This plot is derived from [14].

**Table 2**  
Parameters for the exposure test at 150 °C under oxidising conditions.

Parameter	Parameter value
Water temperature	150 °C
Pressure	50 bar
Conductivity (at 25 °C)	0.06 µS/cm (of feed water to the loop)
High pressure feed water flow	8 kg/h
H <sub>2</sub> O <sub>2</sub>	2400 ppb (In feed water to the loop)
Dissolved O <sub>2</sub>	Generated by decomposition of H <sub>2</sub> O <sub>2</sub> . Measured level in effluent 300–900 ppb
CuCrZr Specimen	ID Ø 12 mm, length 100.6 mm
Flow velocity at 150 °C	8.3 m/s
Exposure time at 150 °C	739 h

**Table 3**  
Parameters for the exposure test at 250 °C under oxidising conditions.

Parameter	Parameter value
Water temperature	250 °C
Pressure	80 bar
Conductivity (at 25 °C)	0.06 µS/cm (of feed water to the loop)
High pressure feed water flow	8 kg/h
Dissolved O <sub>2</sub> in effluent	5000 ppb
CuCrZr Specimen	Reference: ID Ø 12 mm, length 43.4 mm With swirl tape: ID Ø 12 mm, length 42.0 mm Length of swirl tape inside tube 32.0 mm,
Flow velocity at 250 °C	9 to 10 m/s
Exposure time at 250 °C	425 h

**Results**

*Level of corrosion products in the effluent*

The analysis of the content of corrosion products in the effluent from SHFL and conductivity in the effluent is shown in Table 5. Significant levels of Cr, Cu, Ni, and Mo were observed during oxidising conditions

**Table 4**  
Parameters for the exposure test at 250 °C under reducing conditions.

Parameter	Parameter value
Water temperature	250 °C
Pressure	80 bar
Conductivity (at 25 °C)	0.06 µS/cm (of feed water to the loop)
High pressure feed water flow	8 kg/h
Measured H <sub>2</sub> in effluent	45 ml H <sub>2</sub> /kg H <sub>2</sub> O (STP), i.e., 4 ppm
Dissolved O <sub>2</sub> in effluent	<< 10 ppb
CuCrZr Specimens	Reference: ID Ø 12 mm, length 43.1 mm With swirl tape: ID Ø 12 mm, length 42.3 mm Length of swirl tape inside tube 28.9 mm
Flow velocity at 250 °C	8 to 9 m/s
Exposure time at 250 °C	828 h

**Table 5**  
Range of conductivity and content of dominating corrosion products analysed in the effluent from SHFL during the exposure tests.

Parameter	150 °C under oxidising conditions	250 °C under oxidising conditions	250 °C under reducing conditions
Conductivity (µS/cm)	0.3–1.4	1.2–2.2	0.3–0.4
Cr content (ppb)	6	62–73	0.04–0.3
Cu content (ppb)	14	32–45	2–3
Fe content (ppb)	N.D.*	N.D.* – 4	22–28
Mo content (ppb)	0.7	7–16	0.7–0.8
Ni content (ppb)	15	4	2–3

\* N.D.: (not detected) corresponding to a level below the reporting limit of the technique.

both at 150 °C and 250 °C. During the oxidising exposure at 150 °C the conductivity exhibited a decreasing trend, where the reported content of corrosion products is representative of the beginning of the test. Under reducing exposure conditions, the overall conductivity in the effluent was lower compared to oxidising conditions at 250 °C. The level of Cu

**Table 6**

Weight reduction during oxidising exposure at 250 °C for the CuCrZr (reference), the CuCrZr (swirl) and the swirl.

Exposure (h)	CuCrZr (reference), g	CuCrZr (swirl), g	Swirl tape, g
0–238	0.2004	0.2398	0.1833
0–425	0.2884	0.4361	0.3666

and Cr in the effluents was decreased significantly as well under reducing conditions, whereas the level of Fe increased.

*Gravimetry*

*Exposure at 150 °C – Oxidising conditions*

For this specimen the weighing was performed before and after the complete exposure. During the exposure of 739 h, the weight of the specimen was reduced by 0.2196 g. The corresponding decrease of the wall thickness was calculated to be ≈6.5 μm. The estimated FAC rate would be in the order of ≈80 μm per full power year (fpy) using a linear extrapolation with time.

*Exposure at 250 °C – Oxidising conditions*

Gravimetry was performed at an intermediate point in time during the exposure for all specimens, including the swirl tape (Table 6). Based on the gravimetry results the reduction of wall thickness is plotted as a function of exposure time in Fig. 6. The swirl tape experienced the largest reduction of wall thickness. It was calculated as reduction on a single side of the swirl tape, to be comparable to the tubular specimens. The CuCrZr tube with the swirl tape inserted during the exposure exhibited a significantly higher reduction of wall thickness compared to the CuCrZr reference tube exposed without a swirl tape inserted. The reduction of wall thickness for the CuCrZr reference tube was almost ≈20 μm during the 425 h of exposure. Using a linear extrapolation with time the corresponding FAC rate would be in the order of ≈400 μm/fpy for the CuCrZr reference tube and ≈600 μm/fpy for a tube with a swirl tape inserted. For comparison, the thickness of the tube wall is 1500 μm.

*Exposure at 250 °C – Reducing conditions*

The gravimetry results for the specimens exposed under reducing conditions are shown in Table 7. The corresponding reduction of wall thickness is plotted as a function of exposure time in Fig. 7. Under reducing conditions, the specimens have slightly gained weight, thus the values are negative, and the corresponding wall thicknesses would have

**Table 7**

Weight reduction during reducing exposure at 250 °C for the CuCrZr (reference), the CuCrZr (swirl) and the swirl.

Exposure (h)	CuCrZr (reference), g	CuCrZr (swirl), g	Swirl tape, g
0–500	–0.0001	–0.0007	–0.0005
0–828	–0.0011	–0.0009	–0.0008

increased by deposition of particles or precipitation of ionic species present in the circulating water in the loop. In absolute numbers, the corresponding change of wall thickness is orders of magnitude lower under reducing conditions compared to oxidising conditions.

*Post exposure examinations*

*Stereo microscopy*

Stereo microscopy was used to analyse sections of the CuCrZr tubes after they had been cut along their length axes. Images of an un-exposed tube section are shown in Fig. 8, where machining marks, probably associated with the extrusion process, are oriented along the axial direction of the tube.

Images of the inside of the exposed tubes are shown from Figs. 9–13. After exposure at 150 °C and oxidising conditions, the inner portion of the CuCrZr tube exhibited a dark-grey surface (Fig. 9). Both the overview picture (Fig. 9a) and the higher magnification images (Fig. 9b-d) give the impression that the surface is rather smooth; the elongated marks from the manufacturing process can still be seen.

The inside of a CuCrZr tube exposed at 250 °C under oxidising conditions is shown in Fig. 10. The inner section exhibits a sub-mm wavy pattern along its entire length axis with randomly distributed orientation of the waves with respect to the flowing water. The axial extrusion marks are no longer visible on the specimen surface. A feature corresponding to the position of the swirl tape that was inserted during exposure can also be observed on the overview images in Fig. 10a. Only the wavy pattern was observed along the length axis (Fig. 11) on the inside of the reference specimen exposed without a swirl tape inserted.

The specimen tubes that were exposed at 250 °C under reducing conditions exhibited very different surface morphologies (Fig. 12 and Fig. 13). In this case the axial markings from manufacturing can still be clearly observed. The internal surfaces are partially covered with scattered darkly imaging streaks and spots. Unlike the grey surface observed for the specimen exposed at 150 °C under oxidising conditions, the dark

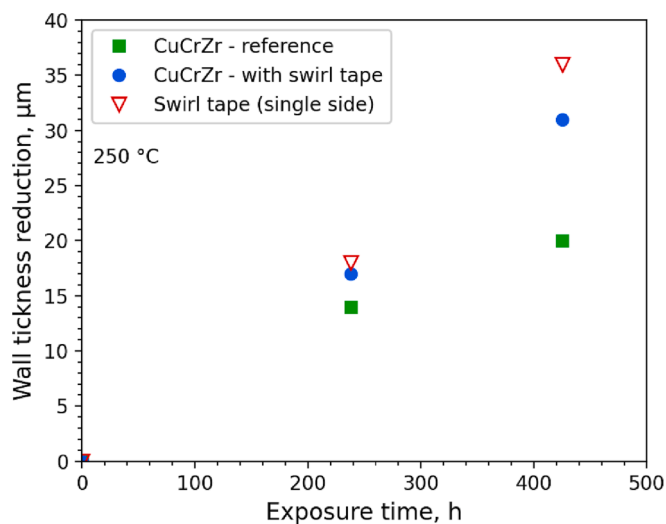


**Fig. 6.** Reduction of wall thickness (in μm) for the CuCrZr tubes at 250 °C under oxidising conditions with and without a swirl tape inserted. For comparison the reduction of wall thickness of the swirl tape is shown as well.

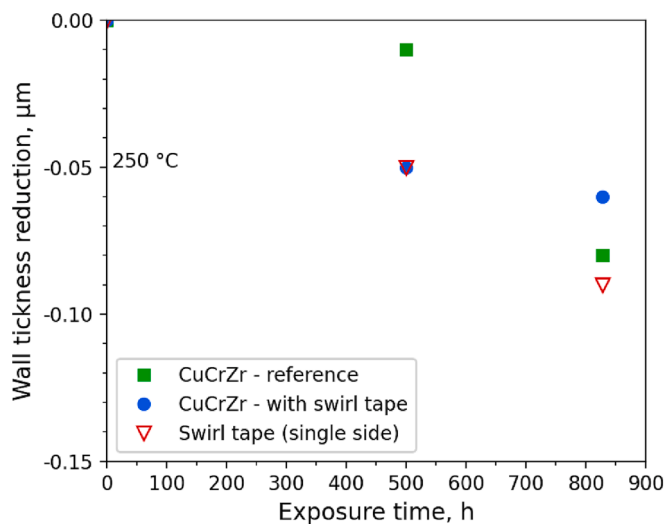


**Fig. 7.** Reduction of wall thickness (in μm) for the CuCrZr tubes at 250 °C under reducing conditions with and without a swirl tape inserted. For comparison the reduction of wall thickness of the swirl tape is shown as well.

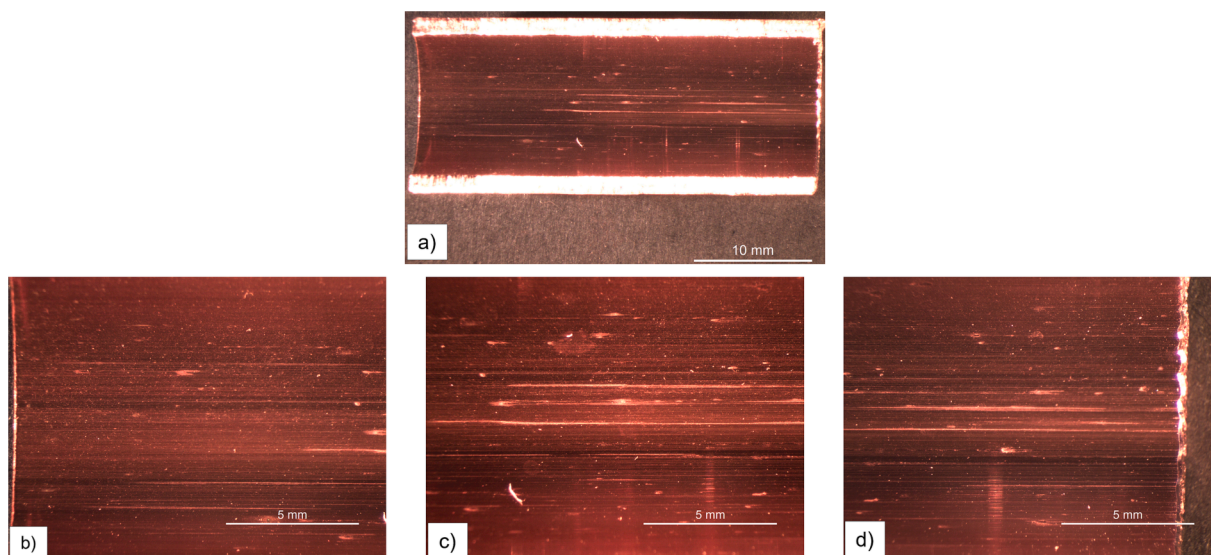


Fig. 8. (a) Overall stereo microscopy image of an un-exposed CuCrZr tube. Higher magnification images showing the (b) left, (c) central and (d) right section of the CuCrZr tube section.

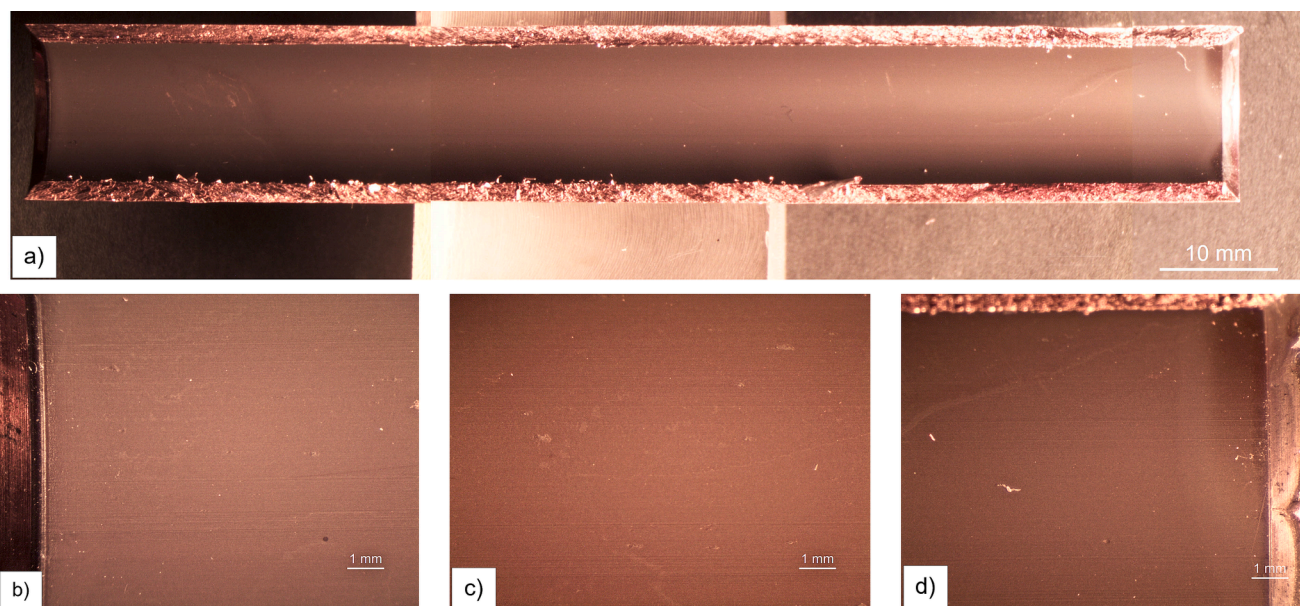


Fig. 9. (a) Overview stereo microscopy image of CuCrZr tube exposed at 150 °C under oxidising conditions. Higher magnification images showing the (b) left, (c) central and (d) right section of the CuCrZr tube section. The flow during exposure was from left (b) to right (d).

grey streaks and spots appeared to be less adherent to the metal substrate, and partially fell off during handling of the specimens. On the larger scale the black streaks are mainly observed on the left of Fig. 12a, showing the specimen that was fitted with swirl tape. In the higher magnification images, the black dots or particles are visible along the extrusion marks associated with the tube manufacturing.

Scanning electron microscopy

Further SEM analyses were performed to obtain an insight regarding the faster FAC rate under oxidising conditions of the specimen exposed at 150 °C.

The oxide morphology is observed to be heterogeneous, as shown in the topography SE image in Fig. 14. In this figure the vertical direction is aligned with the water flow direction in the tube. The oxide has mottled contrast suggesting globular oxide on the scale of < 1 μm. There are secondary features in the oxide, highlighted by red or blue arrows in

Fig. 14. The red solid horizontal arrows point to linear features that align with the water flow direction. The blue dotted vertical arrows point to globular features (≈ tens of microns). Depressions on the order of 1–7 μm (yellow arrows) are observed and are likely to correspond to fall-out of the ‘large’ globular features (blue vertical dotted arrows), followed by further slightly increased material release rates at those drop-out sites.

SEM-EDX analysis was performed in a different region of the specimens, and the associated chemical compositional maps for Cu, Cr, Zr and O are shown in Fig. 15. The SEM-EDX element maps demonstrate that the linear features are rich in Cr; however, spheroidal Cr particles are also identified. Particles rich in Zr appear to be smaller and more spherical. The area fraction of Cr- and Zr-rich precipitates in the oxide is higher than the area fraction of Cr- and Zr-rich precipitates in the bulk material.

Detailed SEM-EDX analyses were performed on the CuCrZr tube with the swirl tape exposed at 250 °C under reducing conditions, in order to

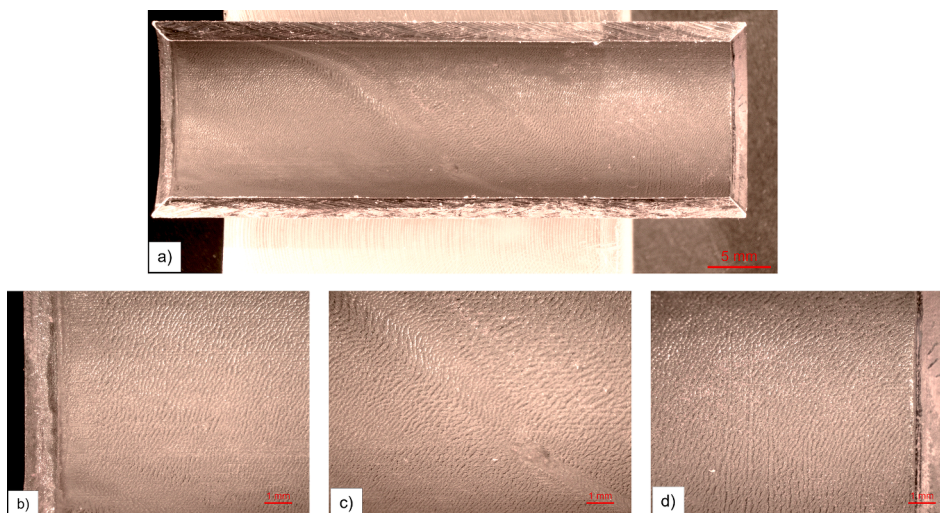


**Fig. 10.** (a) Overview stereo microscopy image of the CuCrZr tube with the swirl tape after exposure at 250 °C under oxidising conditions. Higher magnification images showing the (b) left, (c) central and (d) right section of the CuCrZr tube section. The flow during exposure was from left (b) to right (d).

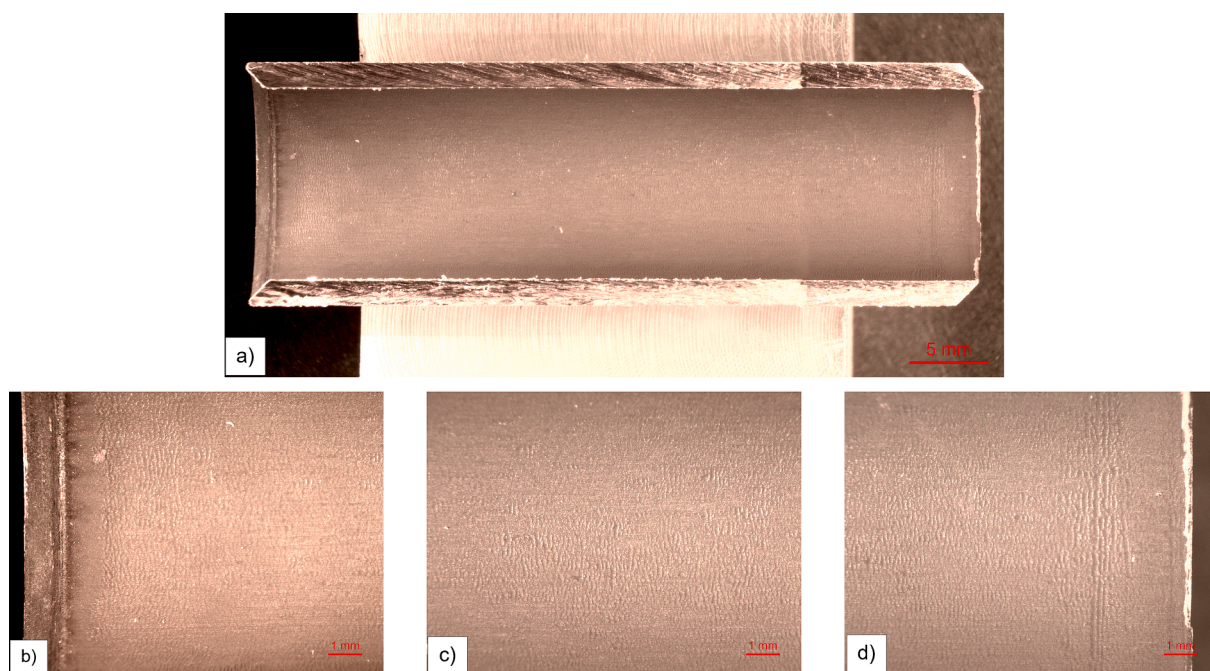


**Fig. 11.** (a) Stereo microscopy images of the CuCrZr tube (reference) after exposure at 250 °C under oxidising conditions. Higher magnification images showing the (b) left, (c) central and (d) right section of the CuCrZr tube section. The flow during exposure was from left (b) to right (d).

explain the apparent weight gain observed in the plot of Table 7. The inner surface of the specimens appears to be decorated with rough and elongated porous deposits that fill the extrusion marks formed during the machining process (Fig. 16a-b), and detailed FIB cross sections confirm the porous nature of the deposits (Fig. 16a-b). Moreover, the inner surface of the CuCrZr tube appears to be covered with a thin (nm) darkly-imaging layer that can be associated with a surface oxide layer. This layer was, however, formed after the FAC test as the specimen came into contact with air, since the reducing ECP during exposure in the loop would have prevented oxidation of Cu [15,16]. Interestingly, the extrusion process induced the formation of an ultrafine-grained layer with the presence of nanometre-scale grains just beneath the inner surface of the specimen. SEM-EDX analyses in Fig. 17a and b show that the corrosion deposits are mainly dominated by Fe. However, numerous other elements such as Cu, Na, Ca, Ni and Si are identified on the inner

surface of the CuCrZr tubes as well. Elements such as Al, Ca, and Si, probably originated from reinforcement fibres present in the bearings of the recirculation pump; moreover, it is worth noting that the surface chemical composition varied from area to area, showing a non-homogenous distribution of the corrosion deposits.

## Discussion

This work involved the study of the FAC on CuCrZr alloy tubes that are intended for use in the fusion reactors ITER and DEMO [5]. The tubes were exposed with different environmental and geometrical parameters under either reducing or oxidising conditions.

The different surface morphologies observed after FAC test under several exposure conditions (Figs. 9–11) are associated with electrochemical, hydraulic and temperature effects. Evidently temperature can

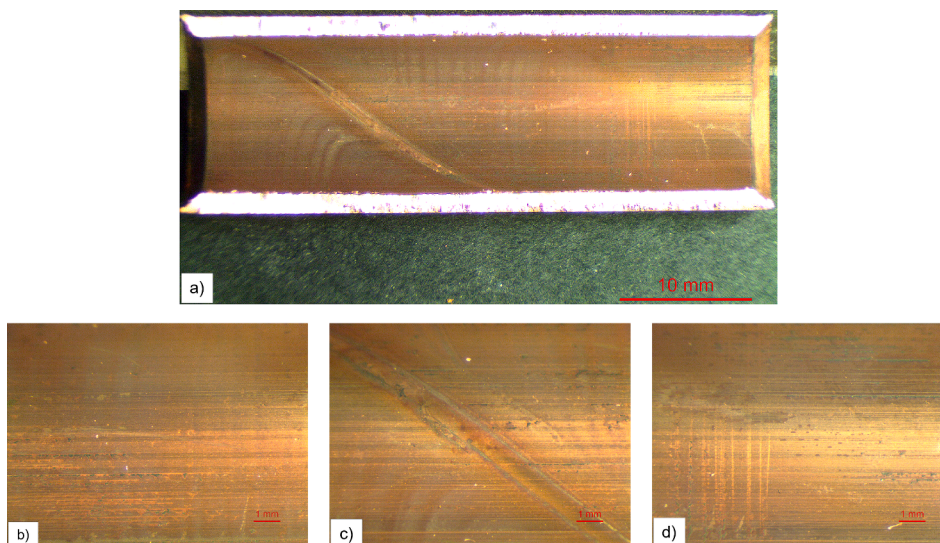


**Fig. 12.** (a) Overview stereo microscopy images of the CuCrZr tube with the swirl tape inserted during exposure at 250 °C under reducing conditions. Higher magnification images showing the (b) left, (c) central and (d) right section of the CuCrZr tube section. The flow during exposure was from left (b) to right (d).

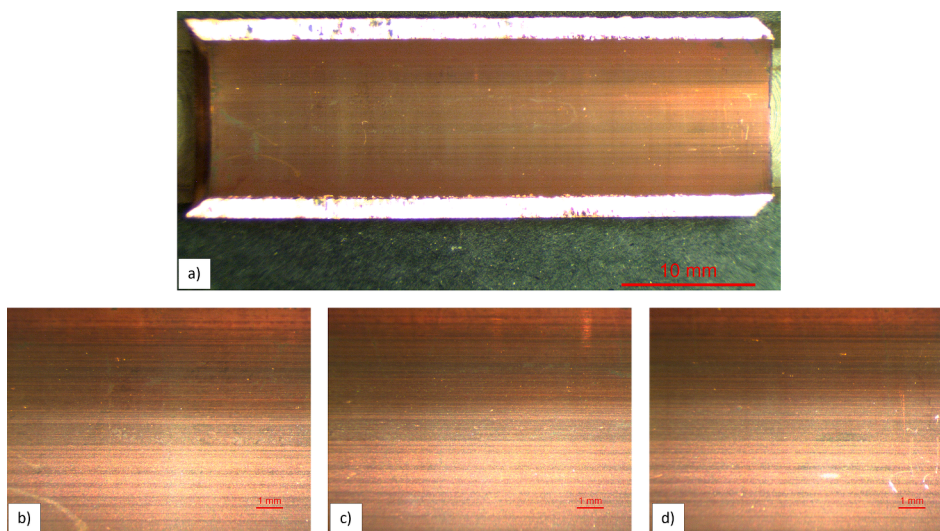


**Fig. 13.** (a) Stereo microscopy images of the CuCrZr tube (reference) after exposure at 250 °C under reducing conditions. Higher magnification images showing the (b) left, (c) central and (d) right section of the CuCrZr tube section. The flow during exposure was from left (b) to right (d).

enhance the FAC attack under oxidising conditions. The fAC-rates based on gravimetry were estimated to be in the order of  $\approx 80 \mu\text{m}/\text{fpy}$  at 150 °C, and  $\approx 400 \mu\text{m}/\text{fpy}$  and  $\approx 600 \mu\text{m}/\text{fpy}$  at 250 °C, depending on whether a swirl tape was inserted in the specimen or not, respectively. For comparison, the wall thickness of the CuCrZr cooling tube is by design 1500  $\mu\text{m}$ . Similar testing of corrosion properties of CuCrZr under rapid flow conditions using the submerged jet impingement technique were reported in [8]. The FAC rate of CuCrZr was observed to be approximately linear with time across the exposure periods examined. A wall thinning of 40  $\mu\text{m}/\text{fpy}$  was reported at oxygenated conditions, 150 °C and a water jet velocity of 10 m/s [8], which is comparable to that observed in this work. At an exposure temperature of 250 °C under oxidising conditions, the jet impingement testing [8] indicated a much higher material release rate, 3500  $\mu\text{m}/\text{fpy}$ , compared to this work. However, the experimental techniques do differ. During submerged jet impingement testing, the flow of water is directed normal to the specimen surface and not parallel to it as during the current exposure. Oxidising conditions at 250 °C have shown to accelerate material loss from CuCrZr also under low flow conditions during exposure of coupon type

specimens in an autoclave [17].

The comparatively rapid material release from the CuCrZr alloy under oxidising conditions can be associated with the oxidation of Cu, which is thermodynamically favourable under these conditions [15,16]. Eventual oxides, such as CuO, are apparently non-protective and non-adherent [8,18]. This can be observed from the SE micrographs in Fig. 14 and Fig. 15, where the release of the oxidized Cu from the matrix has exposed the Cr- and Zr-rich precipitates present in the alloy. The release of Cu-rich corrosion products under oxidising conditions was also confirmed by ICP-MS (Table 5). The coupling of the CuCrZr tubes with the stainless steel 316L tubes in the loop could hypothetically have resulted in galvanic effects and enhanced corrosion release of Cu. Due to the limited conductivity of the fluid in the loop, such attack would have been localized to the very contact point between the alloys [19]. Such attack was however not observed on the CuCrZr specimen in the Figs. 9–11.

The overall conductivity in the effluent was much higher under oxidising conditions than expected, see Table 5. From previous experience, operation of an autoclave at the same temperature and oxidising

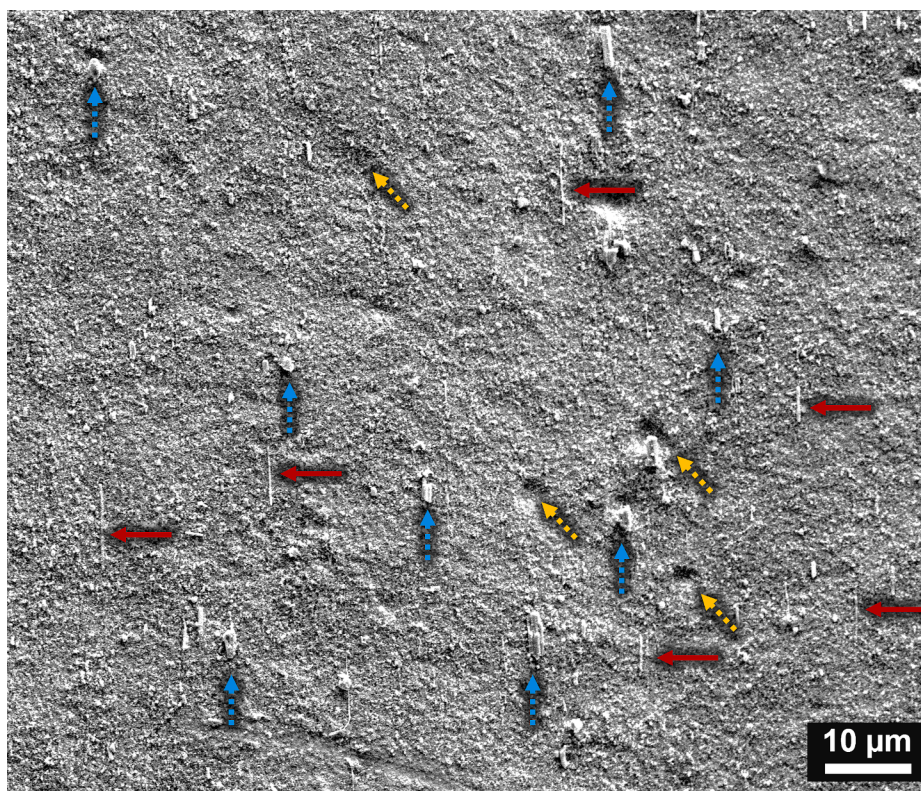


**Fig. 14.** Top view secondary electron (topography) image of oxide in CuCrZr tube. Red solid horizontal arrows show linear features that align with the water flow direction. Blue dotted vertical arrows show large globular features, and yellow arrows shows the depressions associated with the fall-out of the large features. (For interpretation of the references to colour in this figure legend, the reader is referred to the web version of this article.)

conditions would have resulted in an outlet conductivity similar to what is expected in a boiling water reactor, *i.e.* close to or slightly above  $0.1 \mu\text{s}/\text{cm}$  [20]. The dominating metallic corrosion products under oxidizing exposure conditions, except for Cu, were Cr, Ni and Mo. These elements are alloying elements of stainless steel 316L, that is used for the wetted surfaces of the loop system. Before the first exposure the loop system had been pre-passivated in high temperature water to reduce the initial metal release. Under oxidising conditions Cr is rather soluble in high temperature water [21,22]. Low release rates of corrosion products from stainless steel in oxidising conditions relies on the formation of a layered oxides structure [22–24]. This process could hypothetically be hampered in the presence of Cu-containing corrosion products in the water, which would explain the higher-than-expected conductivity in the effluent during oxidising conditions.

Exposure of CuCrZr tubes with and without a swirl tape at  $250\text{ }^{\circ}\text{C}$  under reducing conditions resulted in a non-measurable reduction of wall thickness of the specimens – in fact, the gravimetry results indicated a slight weight increase of the specimens during exposure. The surface oxide (Fig. 16) is attributed to the specimen coming into direct contact with air after exposure, and this oxide may have slightly contributed to the weight gain of the specimen (Table 7). The weight gain of the specimen during reducing conditions was attributed to deposition of material, likely corrosion products originating from stainless steel within the extrusion marks (Fig. 16 - Fig. 17). It is worth noting that under reducing conditions, Cu is expected to be thermodynamically stable as a metal in hydrogenated high temperature water [15,16], and therefore the CuCrZr tubes are likely to be more resistant to corrosion, however erosion could occur in rapidly flowing water. This was observed under reducing conditions at  $250\text{ }^{\circ}\text{C}$  when CuCrZr specimens were subjected to water jets with flow velocities in the range  $7.5$  to  $15\text{ m/s}$  impinging at a right angle [8]. At the strike point the hydraulic conditions are however not comparable to flow conditions in a straight tube which was studied in this work. Sampling of water in the effluent

from the loop showed that the dominating corrosion product was Fe but comparatively low levels of Cu were present as well (Table 5). Under reducing conditions, Fe is soluble in high temperature water [22,25], whereas Cr is thermodynamically stable as an oxide. The Cu which was measured in the effluent from the loop during reducing conditions most likely originated from the previous exposures under oxidising conditions.

A reducing water chemistry achieved through injection of  $\text{H}_2$  is the design condition for the cooling system of future fusion devices [7]. The FAC rates presented in this paper achieved under oxidising conditions should thus be viewed as extreme cases which would only appear if the intended suppression of radiolysis in the cooling system is not complete. Employing CuCrZr tubes for conveying coolant in plasma facing components will then rely on maintaining completely reducing exposure conditions, otherwise FAC will occur. Maintaining reducing conditions is, however, not straightforward since  $\text{H}_2\text{O}_2$  is both a primary radiolysis product and a strong oxidizer. Levels of  $\text{H}_2\text{O}_2$  in the range of  $1\text{ ppb}$  might be enough to increase the ECP and therefore promote the oxidization of Cu and FAC (Fig. 5). Such low levels of  $\text{H}_2\text{O}_2$  might be difficult to maintain in plasma facing components even under hydrogenated coolant conditions [10,11]. Additional countermeasures might be needed to lower the ECP such as injection of noble metal catalysts to the cooling water, suppressing formation of oxidising radiolysis products further [7,26]. Another alternative which is considered for DEMO is application of a corrosion resistant coating inside the CuCrZr tubes [5].

## Conclusions

CuCrZr alloy tubes intended for use in the ITER and DEMO fusion reactors were exposed in a high flow velocity loop in order to evaluate the effect of FAC. From this study, the following conclusions can be drawn:

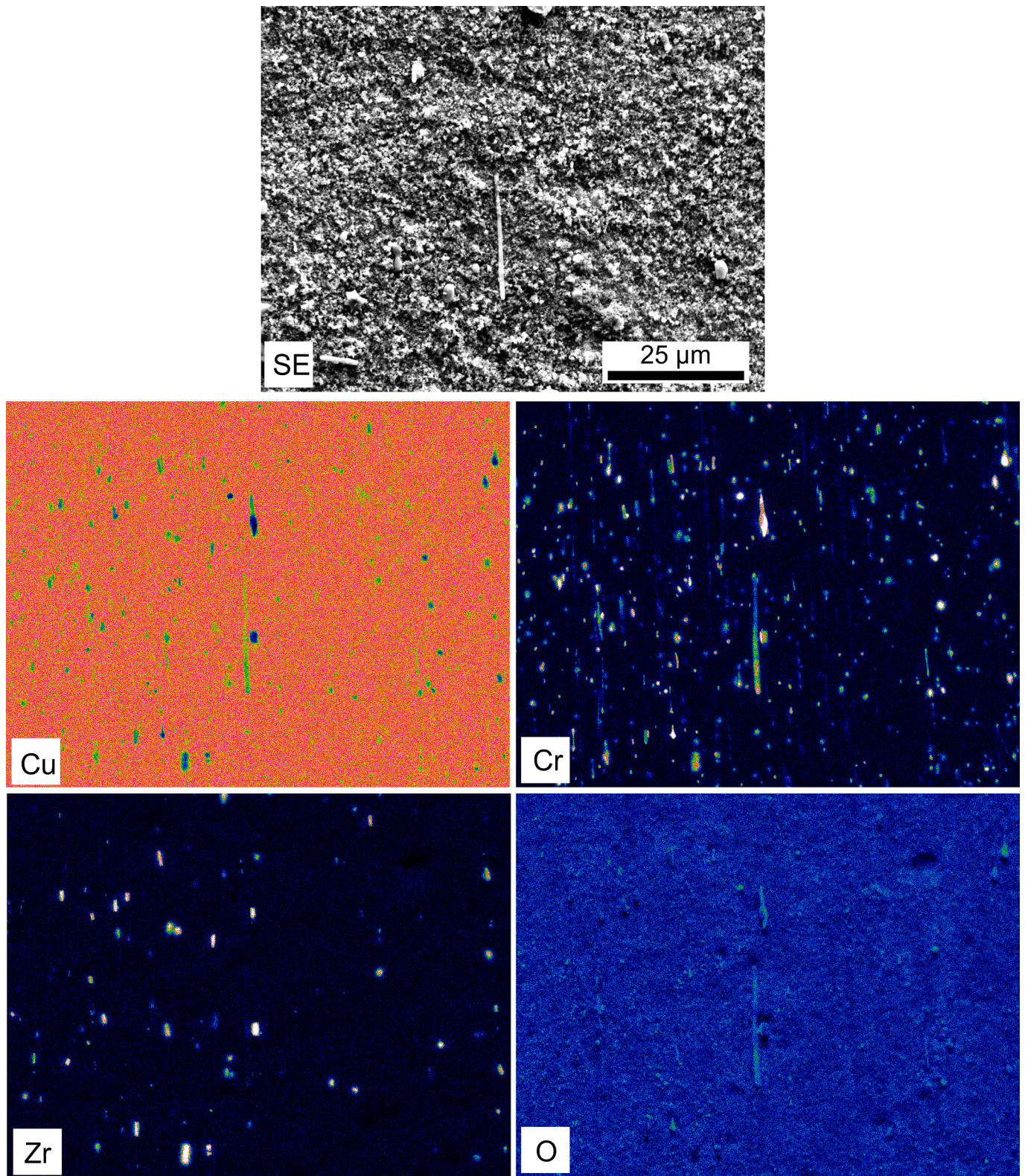


Fig. 15. Chemical maps for Cu, Cr, Zr and O extracted from the SEM-EDX spectrum imaging dataset. Each map is plotted on its individual rainbow scale and shows raw counts for that element (blue: low red: high, white: very high). (For interpretation of the references to colour in this figure legend, the reader is referred to the web version of this article.)

- Exposure of CuCrZr alloy tubes to initially ultrapure water with a flow velocity in the range 8–10 m/s in between 150 °C–250 °C has emphasized the importance of controlling the ECP. The measured FAC rate of the alloy proved to be strongly dependent on whether Cu was thermodynamically stable as a metal under reducing exposure conditions or if an oxidizer was present.
- No FAC attacks were observed on the specimens under reducing conditions. Moreover, minor deposits, probably corrosion products,

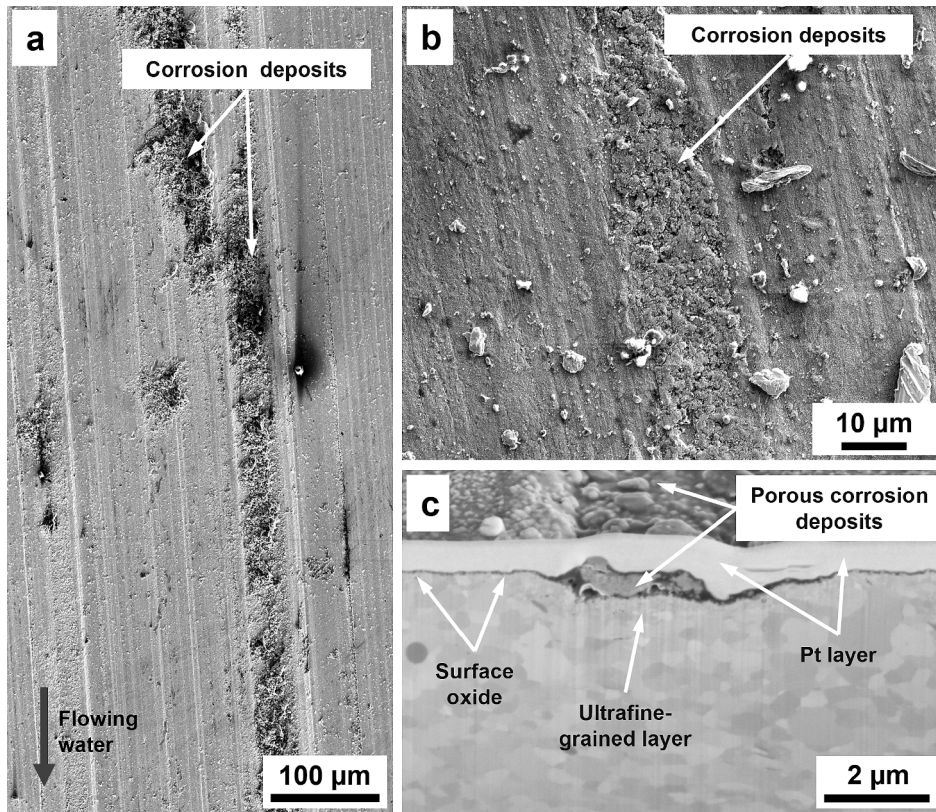


Fig. 16. Top view SE images showing a (a) low magnification portion and (b) a detail of the inner surface of the CuCrZr alloy tube expose at 250 °C under reducing conditions. The porous structure within the extrusion marks is associated with corrosion deposits. (c) Cross section showing the porous corrosion deposits and the formation of a thin darkly-imaging layer that may be associated with a surface oxide layer.

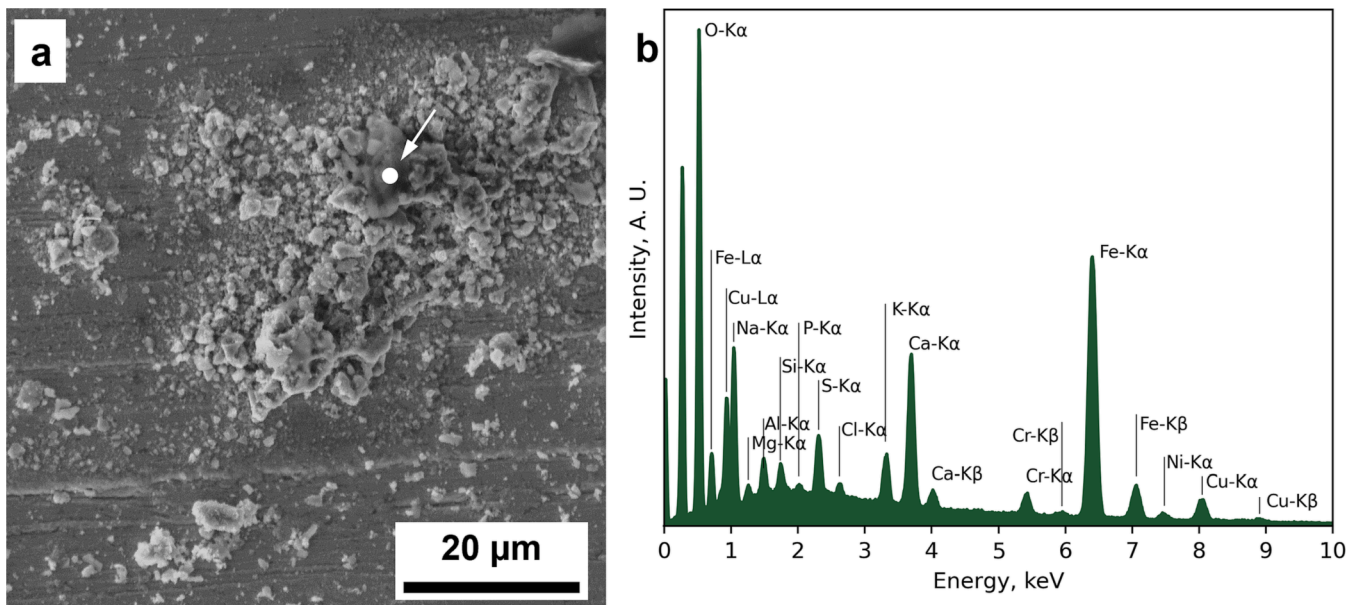


Fig. 17. (a) SE image showing a detail of the inner surface of the CuCrZr alloy exposed at 250 °C under reducing conditions. (b) Associated SEM-EDX spectrum obtained from the point analysis indicated by the white spot in (a).

originating from the stainless steel piping system in the loop, were observed within the extrusion marks on the inner surface of the specimen.

- A FAC rate of  $\approx 400 \mu\text{m}/\text{fpy}$  at 250 °C in the straight CuCrZr tube (without the swirl tape) was extrapolated by the FAC results achieved during testing under oxidising conditions. Employing a swirl

tape inside the tube to enhance turbulence increased the FAC rate up to  $\approx 600 \mu\text{m}/\text{fpy}$  at 250 °C.

- A complete suppression of radiolytically formed oxidising species (e.g.,  $\text{H}_2\text{O}_2$ ) in the cooling systems employing CuCrZr tubes is recommended to avoid FAC. Alternatively, a suitable coating should be

proposed to protect the inner surface of the CuCrZr tubes to prevent FAC.

### CRedit authorship contribution statement

**Johan Öjjerholm:** Methodology, Formal analysis, Investigation, Data curation, Writing – original draft, Supervision, Project administration, Funding acquisition. **Chris Harrington:** Conceptualization, Resources, Writing – review & editing, Supervision, Project administration, Funding acquisition. **Peter Gillén:** Methodology, Software, Validation. **Allan Harte:** Formal analysis, Investigation, Writing – review & editing. **Liberato Volpe:** Formal analysis, Investigation, Writing – review & editing. **Jeong-Ha You:** Conceptualization, Resources, Writing – review & editing, Funding acquisition.

### Declaration of Competing Interest

The authors declare that they have no known competing financial interests or personal relationships that could have appeared to influence the work reported in this paper.

### Data availability

Data will be made available on request.

### Acknowledgment

Several co-workers at Studsvik Nuclear AB are acknowledged for assembling and operating the high flow velocity loop respectively assisting in performing specimen characterisations.

This work has been carried out within the framework of the EUROfusion Consortium, funded by the European Union via the Euratom Research and Training Programme (Grant Agreement No 101052200 – EUROfusion) and from the EPSRC (grant number EP/W006839/1). Studsvik Nuclear AB also acknowledges support from the Swedish Research Council (No. 2017–00643) for adapting SHFL to FAC studies. Views and opinions expressed are however those of the author(s) only and do not necessarily reflect those of the European Union, the European Commission, or the Swedish Research Council. Neither the European Union, the European Commission nor the Swedish Research Council can be held responsible for them.

### References

- [1] J.-H. You, Copper matrix composites as heat sink materials for water-cooled divertor target, *Nucl. Mater. Energy*. 5 (2015) 7–18, <https://doi.org/10.1016/j.nme.2015.10.001>.
- [2] J.H. You, E. Visca, C. Bachmann, T. Barrett, et al., European DEMO divertor target: Operational requirements and material-design interface, *Nucl. Mater. Energy*. 9 (2016) 171–176, <https://doi.org/10.1016/j.nme.2016.02.005>.
- [3] J.H. You, E. Visca, T. Barrett, B. Bös-wirth, et al., European divertor target concepts for DEMO: Design rationales and high heat flux performance, *Nucl. Mater. Energy*. 16 (2018) 1–11, <https://doi.org/10.1016/j.nme.2018.05.012>.
- [4] J.H. You, E. Visca, T. Barrett, B. Bös-wirth, et al., High-heat-flux technologies for the European demo divertor targets: State-of-the-art and a review of the latest testing campaign, *J. Nucl. Mater.* 544 (2021), 152670, <https://doi.org/10.1016/j.jnucmat.2020.152670>.
- [5] J.H. You, G. Mazzone, E. Visca, H. Greuner, et al., Divertor of the European DEMO: Engineering and technologies for power exhaust, *Fusion Eng. Des.* 175 (2022), 113010, <https://doi.org/10.1016/j.fusengdes.2022.113010>.
- [6] J.H. You, G. Mazzone, E. Visca, C. Bachmann, et al., Conceptual design studies for the European DEMO divertor: Rationale and first results, *Fusion Eng. Des.* 109–111 (2016) 1598–1603, <https://doi.org/10.1016/j.fusengdes.2015.11.012>.
- [7] C. Harrington, A. Baron-Wiechec, R. Burrows, R. Holmes, et al., Chemistry and corrosion research and development for the water cooling circuits of European DEMO, *Fusion Eng. Des.* 146 (2019) 478–481, <https://doi.org/10.1016/j.fusengdes.2018.12.095>.
- [8] C. Obitz, J. Öjjerholm, S. Wikman, E. Bratu, Erosion corrosion of CuCrZr specimens exposed for simulated ITER operational conditions, *Nucl. Mater. Energy*. 9 (2016) 261–266, <https://doi.org/10.1016/j.nme.2016.05.001>.
- [9] M. Shimada, B.J. Merrill, Tritium decay helium-3 effects in tungsten, in: 22<sup>nd</sup> International Conference on Plasma Surface Interactions in Controlled Fusion Devices. Rome, Italy, 2016.
- [10] R. Holmes, R. Burrows, S. Dickinson, W.S. Walters, et al., Chemistry and corrosion in the irradiated cooling circuits of a prototype fusion power station, in: The 21<sup>st</sup> International Conference on Water Chemistry in Nuclear Reactor Systems. San Francisco, CA, USA, 2018.
- [11] A. Petrov, D.D. Macdonald, G.R. Engelhardt, Assessment of radiolysis in tokamak cooling water systems of ITER fusion reactor, in: International Conference on Water Chemistry in Nuclear Reactor Systems. San Francisco, CA, USA, 2018.
- [12] P.A. Di Maio, S. Garitta, J.H. You, G. Mazzone, et al., Thermal-hydraulic behaviour of the DEMO divertor plasma facing components cooling circuit, *Fusion Eng. Des.* 124 (2017) 415–419, <https://doi.org/10.1016/j.fusengdes.2017.02.025>.
- [13] J.D. Hunter, Matplotlib: A 2D Graphics Environment, *Comput. Sci. Eng.* 9 (2007) 90–95, <https://doi.org/10.1109/MCSE.2007.55>.
- [14] M. Ullberg, K. Gott, J. Lejon, G. Granath, Advanced ECP model for BWRs, in: 13<sup>th</sup> International Conference on Environmental Degradation of Materials in Nuclear Power Systems - Water Reactors. Whistler, B.C. Canada, 2007.
- [15] B. Beverskog, I. Puigdomenech, Revised pourbaix diagrams for copper at 25 to 300 °C, *J. Electrochem. Soc.* 144 (1997) 3476–3483, <https://doi.org/10.1149/1.1838036>.
- [16] C.M. Chen, K. Aral, G.J. Theus, Computer-calculated potential pH diagrams to 300 °C - volume 2: handbook of diagrams, EPRI. Palo Alto, CA, USA, NP-3137-V2 (1983).
- [17] Y.-J. Huang, M. Nakajima, H. Kurotaki, T. Nozawa, The effect of dissolved oxygen respectively dissolved hydrogen on corrosion behavior of CuCrZr alloy in high temperature water, *Nucl. Mater. Energy*. 31 (2022) 1–6, <https://doi.org/10.1016/j.nme.2022.101190>.
- [18] J.H. Zheng, W.F. Bogaerts, P. Lorenzetto, Erosion–corrosion tests on ITER copper alloys in high temperature water circuit with incident heat flux, *Fusion Eng. Des.* 61–62 (2002) 649–657, [https://doi.org/10.1016/S0920-3796\(02\)00256-9](https://doi.org/10.1016/S0920-3796(02)00256-9).
- [19] D.A. Jones, Principles and Prevention of Corrosion. Upper Saddle River, NJ, USA: Prentice-Hall, 1996.
- [20] S.E. Garcia, J.F. Giannelli, J.A. Tangen, J.A. Jarvis, et al., Water Chemistry Control Guidance and Technologies for New Design Boiling Water Reactors, in: International Conference on Water Chemistry of Nuclear Reactor Systems. Brighton, UK, 2016.
- [21] B. Beverskog, I. Puigdomenech, Revised pourbaix diagrams for chromium at 15–300 °C, *Corros. Sci.* 39 (1997) 43–57, [https://doi.org/10.1016/S0010-938X\(97\)89244-X](https://doi.org/10.1016/S0010-938X(97)89244-X).
- [22] B. Beverskog, I. Puigdomenech, Pourbaix diagrams for the ternary system of iron-chromium-nickel, *Corros.* 55 (1999) 1077–1087, <https://doi.org/10.5006/1.3283945>.
- [23] J. Robertson, The mechanism of high temperature aqueous corrosion of stainless steels, *Corros. Sci.* 32 (1991) 443–465, [https://doi.org/10.1016/0010-938X\(91\)90125-9](https://doi.org/10.1016/0010-938X(91)90125-9).
- [24] J. Chen, H. Bergqvist, D. Jäder-näs, G. Granath, High resolution electron microscopy study on the thin oxide films formed on type 316L stainless steel exposed under simulated BWR water chemistry environments, in: 14<sup>th</sup> International Conference on Environmental Degradation of Materials in Nuclear Power Systems - Water Reactors. Virginia Beach, VA, USA, 2009.
- [25] B. Beverskog, I. Puigdomenech, Revised pourbaix diagram for iron at 25–300 °C, *Corros. Sci.* 38 (1996) 2121–2135, [https://doi.org/10.1016/S0010-938X\(96\)00067-4](https://doi.org/10.1016/S0010-938X(96)00067-4).
- [26] Y.J. Kim, L.W. Niedrach, P.L. Andresen, Corrosion potential behavior of noble metal-modified alloys in high-temperature water, *Corros.* 52 (1996) 738–743, <https://doi.org/10.5006/1.3292066>.